Strong-field control of x-ray absorption

R Santra, C Buth, E R Peterson, R W Dunford, E P Kanter, B Krässig, S H Southworth and L Young

Argonne National Laboratory, Argonne, Illinois 60439, USA

E-mail: rsantra@anl.gov

Abstract. Strong optical laser fields modify the way x rays interact with matter. This allows us to use x rays to gain deeper insight into strong-field processes. Alternatively, optical lasers may be utilized to control the propagation of x rays through a medium. Gas-phase systems are particularly suitable for illustrating the basic principles underlying combined x-ray and laser interactions. Topics addressed include the impact of spin-orbit interaction on the alignment of atomic ions produced in a strong laser field, electromagnetically induced transparency in the x-ray regime, and laser-induced alignment of molecules.

1. Introduction

In x-ray science, cross sections for x-ray absorption in matter are typically assumed to be invariants, depending only on the atomic composition of the material [1, 2]. However, by utilizing electromagnetic fields, it is possible to modify x-ray absorption cross sections in a controlled way. Wuilleumier and Meyer [3] review combined laser/x-ray experiments performed at laser intensities that are small in comparison to an atomic unit ($\sim 10^{16}$ W/cm^2), so that the laser–matter interaction may be described perturbatively. As discussed in reference [4], at laser intensities above $\sim 10^{10}$ W/cm^2, interesting processes such as tunnel ionization [5] and molecular alignment [6] can occur. In the following, we discuss three different scenarios for modifying x-ray absorption near an inner-shell edge. Strong-field ionization at 10^{14} W/cm^2 is the topic of section 2. In section 3, laser dressing at 10^{13} W/cm^2 is discussed. Section 4 presents results of a recent joint theoretical and experimental study on x-ray absorption by laser-aligned molecules (10^{12} W/cm^2). For the purpose of this paper, the x-ray regime is defined by photon energies that are sufficient to produce, via photoabsorption, inner-shell vacancies in atoms such as carbon or heavier. This definition includes both soft [1] and hard [2] x rays. We concentrate on a laser wavelength of 800 nm. In this paper, the laser and x-ray fields are assumed to be linearly polarized and co-propagating.

2. X-ray probe of strong-field ionized atoms

Reference [7] develops an x-ray microprobe methodology that allows one to study strong-field ionized atoms or molecules using x-ray absorption spectroscopy. X rays are focused within the focal volume of a strong optical field such that the x-ray focal width is much smaller (by a factor of 10 in reference [7]) than the laser focal width. X-ray absorption is monitored by measuring the x-ray fluorescence resulting from inner-shell hole formation within an interval along the laser propagation axis that is short in comparison with the Rayleigh range [7]. Thus, the x-ray microprobe methodology reduces averaging effects over the spatial intensity distribution of the

laser field. The species first studied in the strong-field experiments carried out at Argonne's Advanced Photon Source was krypton [7, 8].

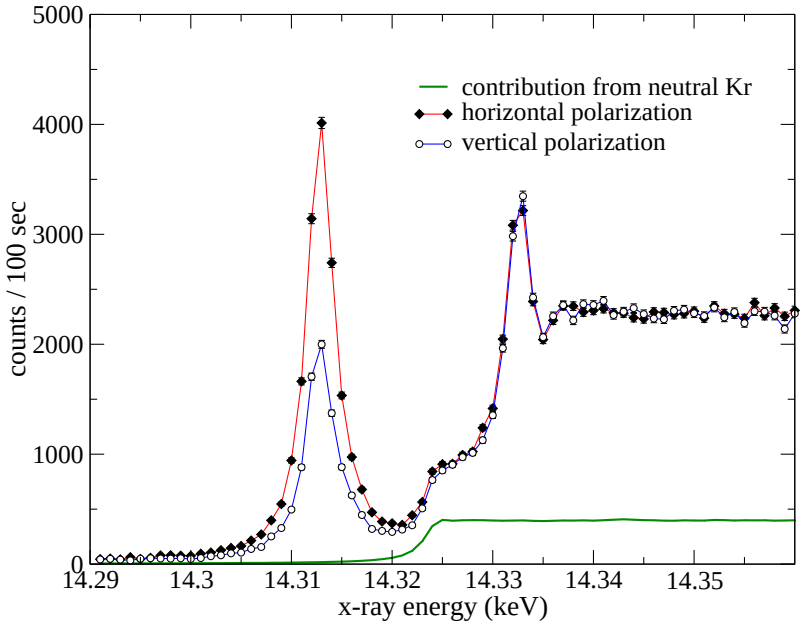

Figure 1. Experimental near-K-edge absorption spectra of strong-field ionized Kr. Data are shown for both parallel and perpendicular laser and x-ray polarizations. Also depicted is the background contribution from neutral Kr.

Figure 1 shows the Kr $K\alpha$ fluorescence signal from krypton gas in a gas cell (number density 5×10^{15} cm^{-3}) as a function of the energy of the absorbed x-ray photon. The signal was measured 0.5 ns after a 50-fs, $\sim 10^{14}$-W/cm^2 laser pulse ionized the Kr atoms. The full diamonds/red lines show the fluorescence signal for laser polarization parallel to the x-ray polarization; the open circles/blue lines refer to perpendicular polarization directions. For the case shown, the majority of atoms are ionized. There are two prominent features in the spectrum resulting from Kr^+ $1s \rightarrow 4p$ and $1s \rightarrow 5p$ excitations. The contribution of fluorescence from neutral atoms in the interaction region is indicated by the green line. The ratio of ions to neutrals is about 4.7 : 1. It may be concluded from the spectrum shown that there is very little Kr^{2+} present, because the well-separated Kr^{2+} $1s \rightarrow 5p$ excitation line seen at higher laser intensities in reference [7] is hardly noticeable here.

There are two interesting observations we would like to point out. First, strong-field ionization modifies the structure observed in the near-edge absorption spectrum quite dramatically. For instance, when Kr spectra are measured in the absence of the laser, there is very little absorption at an x-ray photon energy of 14.313 keV. In the presence of the laser, there appears at this photon energy the strong Kr^+ $1s \rightarrow 4p$ absorption resonance seen in figure 1. (See reference [9] for a similar observation made in potassium.) The effect is very pronounced, but the disadvantage of this form of strong-field control of x-ray absorption is that it is not rapidly reversible: One has to wait until the laser-produced plasma has expanded [8] and neutral atoms have filled the original plasma volume.

The second observation is that the Kr^+ $1s \rightarrow 4p$ resonance displays a strong dependence on the relative polarization of laser and x rays. The resonant x-ray absorption cross section for parallel polarizations is two times larger than in the perpendicular case. The observed linear dichroism provides information on the alignment of the $4p$ hole orbital produced by the strong laser pulse [7, 10]. The hole orbital is aligned along the laser polarization axis, which defines the quantization axis. As shown in references [7, 10], in order to understand the observations, it is necessary to take into account the effect of spin-orbit coupling. Nonrelativistic tunneling or multiphoton ionization models strongly overestimate the degree of ion alignment. According

Table 1. Kr^+ quantum state populations $\rho_{j,|m|}$, following strong-field ionization of Kr, obtained from experiment and theory. The errors shown reflect only statistical uncertainties (2σ). Potential systematic errors are not included.

	$\rho_{3/2,1/2}$ (%)	$\rho_{1/2,1/2}$ (%)	$\rho_{3/2,3/2}$ (%)
Experimental	59 ± 6	35 ± 4	6 ± 6
Theoretical	71	25	4

to adiabatic strong-field ionization calculations that include spin-orbit coupling [10], there is hardly any mixing between the $4p_{3/2}$ and $4p_{1/2}$ orbitals at the electric-field strength at which Kr ionizes. In other words, the laser field is not strong enough to break spin-orbit coupling. The same is true in the case of strong-field ionization of Xe [11]. Therefore, if there are coherences in the density matrix of Kr^+ or Xe^+, they are not caused by the strength of the laser electric field.

In reference [11] it was demonstrated for Xe that inner-shell absorption spectra of laser-produced ions may be used to determine the quantum state populations $\rho_{j,|m|}$, i.e., the probability to find an ion with a hole in the np_j orbital with projection quantum number $\pm m$ (n is the principal quantum number of the valence shell). In table 1, we present the results of such an analysis for Kr. The analysis is based on the fact that using standard angular momentum algebra, it may be shown for the $1s \rightarrow 4p$ transition in Kr^+ that the x-ray absorption cross sections for parallel ($\parallel$) and perpendicular ($\perp$) polarizations are given by

$$\sigma_{\parallel} = 2\rho_{3/2,1/2}\sigma_{3/2} + \rho_{1/2,1/2}\sigma_{1/2}, \tag{1}$$

$$\sigma_{\perp} = \frac{1}{2}\{\rho_{3/2,1/2} + 3\rho_{3/2,3/2}\}\sigma_{3/2} + \rho_{1/2,1/2}\sigma_{1/2}. \tag{2}$$

Using *ab initio* values for the m-averaged cross sections $\sigma_{3/2}$ ($1s \rightarrow 4p_{3/2}$) and $\sigma_{1/2}$ ($1s \rightarrow 4p_{1/2}$) [12], equations (1) and (2) may be fitted to the experimental data to determine the $\rho_{j,|m|}$. As may be seen in table 1, the adiabatic strong-field ionization model we use [10] reproduces the general trend displayed by the experimental quantum state populations.

3. X-ray absorption by laser-dressed atoms

We now turn our attention to x-ray absorption by noble-gas atoms in a laser field of intensity 10^{13} W/cm^2 or lower [13, 14]. In this regime, both inner-shell and valence electrons in the electronic ground state remain essentially unperturbed (this applies particularly to light atomic species such as neon). The primary effect of the laser field on x-ray absorption is to modify ("dress") the inner-shell-excited electronic states in the vicinity of an inner-shell edge. Therefore, this laser-dressing approach to strong-field control of x-ray absorption is reversible and leaves the target intact. We assume in this section that the laser and x-ray polarizations are parallel.

The reason why high intensities are required in order to observe laser-dressing effects in the x-ray absorption spectrum is easy to understand. The Rabi frequencies associated with laser coupling of the inner-shell-excited states must be larger than the decay widths of these states. Inner-shell-excited atoms, which relax via Auger decay and/or x-ray fluorescence, decay at least a thousand times faster than valence-excited atoms. Thus, since the dipole coupling matrix elements between Rydberg levels are similar in the valence- and inner-shell-excited cases, the laser intensity must be at least 10^6 times higher than what is needed when all electromagnetic fields involved are in the optical regime.

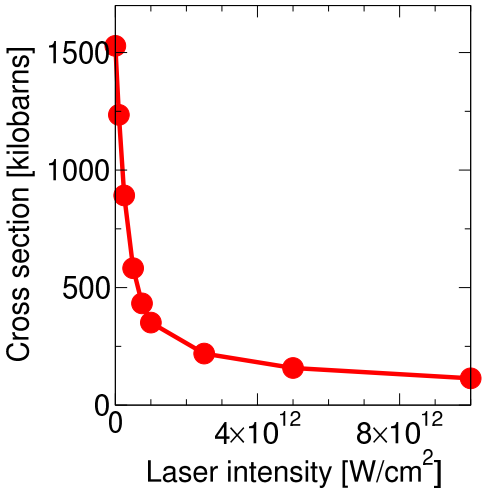

Figure 2. Calculated dependence of the $1s \rightarrow 3p$ x-ray absorption cross section of Ne on the intensity of the dressing laser. The laser and x-ray polarizations are assumed to be parallel.

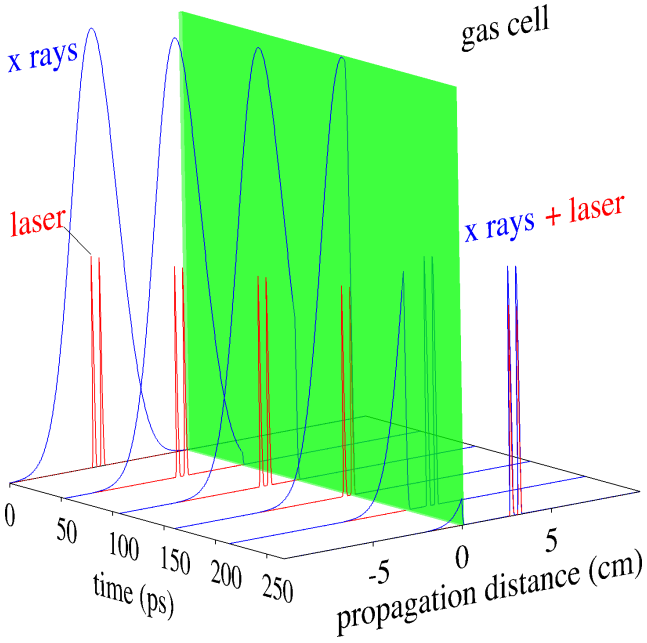

Figure 3. Generation of ultrafast x-ray pulses using laser dressing of Ne. See the text for details.

An *ab initio* theory for calculating the x-ray absorption spectrum of an atom exposed to an intense laser field is developed in Ref. [13]. The method utilizes the Hartree-Fock-Slater approximation [15] to describe the electronic structure of the unperturbed atom. The coupling to the laser is treated nonperturbatively within the strong-field (Floquet [16]) limit of nonrelativistic quantum electrodynamics. The laser-dressed, inner-shell-excited states are calculated by diagonalizing a non-Hermitian Hamiltonian matrix. The x-ray-induced transition from the atomic ground state to the laser-dressed, inner-shell-excited states is treated using perturbation theory. At a laser intensity of 10^{13} W/cm^2, the application of this theory to Kr near the K edge at 14.3 keV demonstrates a $\sim$ 20% suppression of x-ray absorption at the $1s \rightarrow 5p$ transition [13]. The suppression is mainly due to laser coupling of $5p$ to $5s$ and $4d$. In view of the 2.7-eV decay width of K-shell-excited Kr [17], the laser intensity it would take to induce a much stronger modification of the near-K-edge structure of Kr is so high that Kr in its ground state would be strong-field-ionized (cf. section 2).

In neon, the laser-dressing effect is much more dramatic [14]. This is because the decay width of K-shell-excited Ne [18] is smaller than in Kr by a factor of 10. The laser intensity dependence of the x-ray absorption cross section of Ne at the prominent $1s \rightarrow 3p$ transition (867 eV) is displayed in figure 2. Laser dressing at an intensity of 10^{13} W/cm^2 is found to suppress x-ray absorption at the $1s \rightarrow 3p$ resonance by a factor of 13. This suppression of x-ray absorption is a manifestation of electromagnetically induced transparency (EIT) [19–21]. To describe EIT one usually considers three eigenstates of the atom under consideration. To a first approximation in our case, these states are the Ne ground state (level 1), the excited state of Ne with a K-shell hole and an electron in the $3p$ orbital (level 2), and the excited state of Ne with a K-shell hole and an electron in the $3s$ orbital (level 3). The laser creates a coherent superposition of levels 2 and 3, so-called dressed states. At the x-ray photon energy corresponding to the laser-unperturbed $1 \rightarrow 2$ transition, the transition pathways from level 1 to the two dressed states interfere destructively. Hence, over a narrow x-ray energy range of $\sim$ 100 meV, absorption of the x rays is suppressed at the photon energy corresponding to the transition from level 1 to

level 2. Because of the high laser intensity required for EIT in the x-ray domain, the three-level model provides at best a qualitatively correct picture. For instance, at 10^{13} W/cm^2, the laser ionizes the Rydberg electron at a rate that is comparable to the Auger decay rate of the K-shell hole, i.e., there is strong laser coupling to states outside the three-level model space.

The ability to control x-ray absorption in Ne at the $1s \rightarrow 3p$ resonance using a strong laser field allows one to imprint pulse shapes of the optical dressing laser onto the x rays. The idea is illustrated in figure 3. Using a 2-mm long gas cell filled with one atmosphere of neon, an x-ray pulse at the $1s \rightarrow 3p$ resonance energy is practically completely absorbed in the gas cell [14]. The typical duration of an x-ray pulse from a third-generation synchrotron is ~ 100 ps. Such an x-ray pulse may be overlapped in time and space with one or several ultrashort, intense laser pulses. Those portions of the x-ray pulse that overlap with the laser are transmitted through the gas cell. In the case shown in figure 3, where the two dressing laser pulses have a peak intensity of 10^{13} W/cm^2, the intensity of the two transmitted x-ray pulses is about 60% of the incoming x-ray intensity. The time delay between the two x-ray pulses can be controlled by changing the time delay between the two laser pulses, opening a route to ultrafast all x-ray pump-probe experiments. With an analogous strategy, controlled shaping of short-wavelength pulses might become a reality. A disadvantage of the method is that it is applicable only at certain x-ray energies.

4. X-ray absorption by laser-aligned molecules

The schemes discussed in sections 2 and 3 rely on modifying the system's electronic structure. In the following, we present a third scheme for controlling resonant x-ray absorption that is conceptually somewhat different. To motivate this scheme, recall from section 2 that Kr^+ ions produced in a strong laser field are aligned along the laser polarization axis. Kr^+ ions and Br atoms are isoelectronic and have essentially the same electronic structure. In contrast to Kr^+, Br forms many molecules. If the open $4p$ shell of Br is not filled upon molecule formation, and if the effective $4p$ hole orbital is aligned with respect to the molecular frame, then the hole orbital may be aligned in space by aligning the molecule.

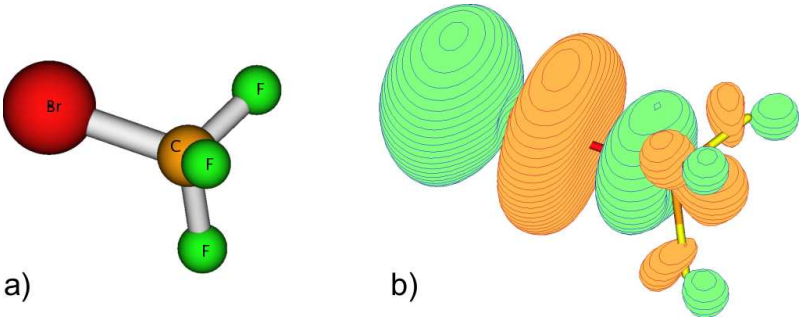

Figure 4. a) Equilibrium geometry of CF_3Br in its electronic ground state. b) Lowest unoccupied molecular orbital of CF_3Br.

The molecule selected for experimental investigations at Argonne's Advanced Photon Source is CF_3Br, which is known as bromotrifluoromethane or halon-1301 [23]. The equilibrium geometry of this molecule in its electronic ground state is shown in figure 4a. A Mulliken population analysis [22] we have performed on the Hartree-Fock ground-state wave function of CF_3Br indicates that the carbon atom carries a partial charge of $+0.71$, whereas the partial charge on each of the three fluorine atoms is -0.23. The Br atom acquires essentially no charge (partial charge of -0.02). It may therefore be expected that the Br hole orbital remains at least partially unoccupied in CF_3Br. This is consistent with the fact that the lowest unoccupied molecular orbital of CF_3Br, which is displayed in figure 4b, is a σ^* orbital with substantial Br $4p_z$ character. Here, z refers to the C-Br axis. The highest occupied molecular orbital of CF_3Br is a doubly degenerate π orbital corresponding to Br $4p_x$ and $4p_y$. Owing to the strong

localization of the Br $1s$ orbital near the Br nucleus, an x-ray-induced transition from the Br K shell to the σ^* orbital probes only the atomic p_z character of the σ^* orbital. Let D_x, D_y and D_z denote the Cartesian components, with respect to the molecular frame, of the transition dipole vector between Br $1s$ and σ^*. The molecule CF_3Br belongs to the C_{3v} point group. Hence, $D_x = D_y = 0$, for Br $1s$ and the σ^* orbital span the irreducible representation A_1. Only when the x-ray polarization vector has a component along the C-Br axis can x-ray absorption at the Br $1s \rightarrow \sigma^*$ resonance take place. Estimates show that the intramolecular electric field in CF_3Br breaks spin-orbit coupling in Br, so that in contrast to the situation we discussed in connection with Kr^+, spin-orbit coupling may be neglected.

The polarization dependence of resonant x-ray absorption by aligned molecules was demonstrated in studies on surface-adsorbed molecules [24] and fixed-in-space molecules [25]. This effect may be exploited for a laser-based control scheme for x-ray absorption. As explained in reference [6] and references therein, small molecules with an anisotropic polarizability may be aligned along the laser polarization axis at laser intensities in the range 10^{11} to 10^{12} W/cm^2. The physics underlying laser-induced molecular alignment is easy to understand: The instantaneous laser electric field polarizes the molecule. The electric dipole moment induced depends on the molecular polarizability tensor and the laser electric field vector with respect to the molecular frame. The interaction of the induced dipole moment with the laser electric field leads to an effective potential for the rotational degrees of freedom of the molecule. The effective laser-induced potential is proportional to the cycle-averaged laser intensity. The potential-energy minimum is reached when the most polarizable molecular axis is parallel to the laser polarization axis. In the case of a symmetric rotor, the molecule-specific quantity that characterizes the effective potential is $\alpha_\parallel - \alpha_\perp$, which is the difference between the polarizability component of the molecule along the molecular symmetry axis and the polarizability component perpendicular to the molecular symmetry axis. An assumption typically made is that the laser photon energy is far too low to electronically excite the molecule via a one-photon transition. Consequently, it is permissible to use the *static* polarizability components obtained in the limit of infinite wavelength. We calculated $\alpha_\parallel - \alpha_\perp$ using coupled-cluster linear response theory [26] and found that for CF_3Br the difference between $\alpha_\parallel - \alpha_\perp$ determined in the static limit and $\alpha_\parallel - \alpha_\perp$ determined at 800 nm is indeed only about 2%.

For the purpose of minimizing temporal averaging effects, it is important that the duration of the molecular alignment is not substantially shorter than the x-ray pulse duration of ~ 100 ps. This means that the impulsive alignment technique [6], where alignment persists for only a few ps, is unsuitable. In the adiabatic regime [6], where the laser intensity envelope changes slowly on the characteristic rotational time scale of the molecule, the alignment persists for as long as the laser pulse is on. CF_3Br is a prolate symmetric top molecule [27] with a rotational period of 239 ps. (This is the characteristic time for rotation about an axis perpendicular to the C-Br axis.) In order to obtain a high laser repetition rate (1 kHz), the laser pulse energies were limited to about 2 mJ with a pulse duration of 95 ps. Even though this is somewhat shorter than the rotational period, we find in our calculations, which are similar to the ones reported in reference [28], that at temperatures of several K or higher, the molecular response to the laser pulse is essentially adiabatic and tracks the laser pulse envelope.

Figure 5 shows a comparison between experimental data taken recently at the Advanced Photon Source and a theory we have developed for this purpose. The peak laser intensity was 0.85×10^{12} W/cm^2. The experimental setup was similar to the Kr experiment mentioned in section 2. $K\alpha$ fluorescence was used to monitor $1s$-hole formation in Br. The Br near-K-edge absorption spectrum was measured and the $1s \rightarrow \sigma^*$ resonance at 13.476 keV was identified. The experimental data plotted in figure 5 were obtained on resonance, after subtraction of a 10% background from inner-shell-excited Rydberg and continuum states that overlap with the resonance. The primary experimental difference from the atomic Kr experiment is that a

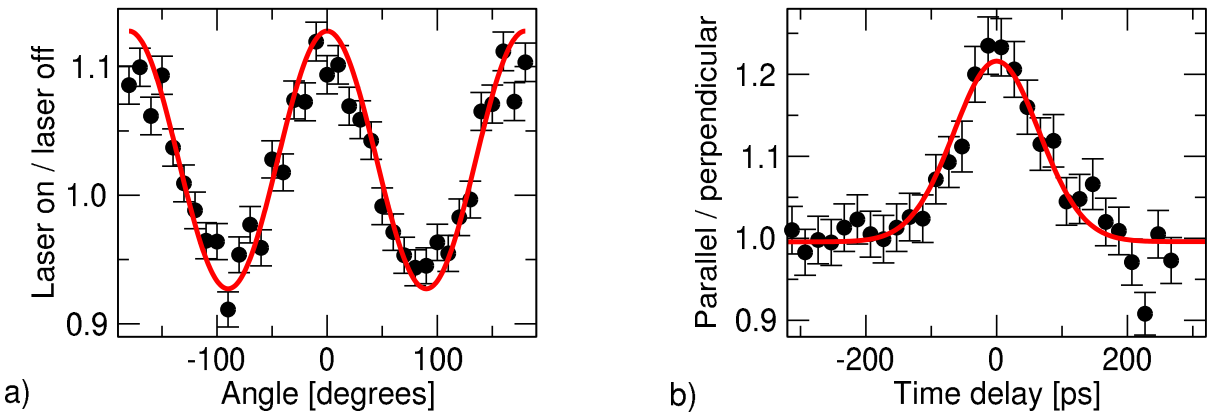

Figure 5. Resonant x-ray absorption by strong-field-aligned CF_3Br. Comparison between theory (solid line) and experiment (circles plus error bars). a) Dependence of the x-ray absorption signal on the angle between the laser and x-ray polarization axes. b) Ratio between x-ray absorption signal for parallel laser and x-ray polarizations and x-ray absorption signal for perpendicular laser and x-ray polarizations, as a function of the time delay between the laser and x-ray pulses.

supersonic expansion of 5% CF_3Br seeded in He was used to produce a cold jet of molecules. By applying a high backing pressure to the nozzle through which the gas mixture expands, a low rotational temperature may be achieved. This is crucial for alignment in the adiabatic regime [6]. In the experiment at the Advanced Photon Source, a backing pressure of up to 9 bar was applied, which by comparison with reference [29] suggests a rotational temperature of the order of 10 K.

The central quantities we calculate for comparison with experiment are on-resonance absorption cross sections for parallel laser and x-ray polarizations ($\sigma_\parallel$); perpendicular laser and x-ray polarizations ($\sigma_\perp$); and a laser-free thermal ensemble ($\sigma_{\rm th}$). Let $J_{\rm X}(t)$ denote the x-ray photon current density (pulse envelope). The x-ray absorption probability per pulse is then given by

$$P_i(\tau) = \int_{-\infty}^{\infty} \sigma_i(t)\, J_{\rm X}(t-\tau)\, {\rm d}t, \qquad i = \parallel, \perp, {\rm th}, \tag{3}$$

where τ is the time delay between the laser and x-ray pulses, which are both assumed to be Gaussian. At $\tau = 0$, the maxima of the laser and x-ray pulses coincide. One quantity that may be measured is the dependence of the x-ray absorption on the angle $\vartheta_{\rm LX}$ between the laser and x-ray polarizations. This is shown in figure 5a ($\tau = 0$), where the ratio between the laser-on and laser-off signals is plotted. The theoretical expression for the $\vartheta_{\rm LX}$ dependence of the laser-on/laser-off ratio is

$$R(\vartheta_{\rm LX}) = \frac{P_\parallel(0)}{P_{\rm th}(0)} \cos^2\vartheta_{\rm LX} + \frac{P_\perp(0)}{P_{\rm th}(0)} \sin^2\vartheta_{\rm LX}. \tag{4}$$

Assuming a rotational temperature of 21 K and an x-ray pulse duration of 127 ps, good agreement is found between experiment and theory. Note, in particular, that the theory correctly predicts that $|R(0^\circ)-1| > |R(90^\circ)-1|$. Figure 5b shows the ratio $P_\parallel(\tau)/P_\perp(\tau)$ as a function of the time delay τ. Agreement between theory and experiment is again satisfactory for a temperature of 21 K and an x-ray pulse duration of 127 ps.

In conclusion, we would like to mention some future challenges and opportunities. We discussed in section 2 a spectroscopic probe of strong-field-ionized noble-gas atoms. The *coherence* properties of the ion density matrix produced in a strong optical field are not known and pose a challenge for future experiments with ultrafast radiation pulses. The EIT effect for x rays explored in section 3 may make it possible to perform ultrafast x-ray pulse shaping. Such pulses could have useful applications in time-resolved x-ray science. Finally, in this section we demonstrated that laser-induced alignment allows one to control resonant x-ray absorption in molecules. Calculations indicate that by reducing the molecular rotational temperature to a few K, and by using an x-ray pulse that is shorter than the aligning laser pulse, it should be possible to suppress x-ray absorption for perpendicular laser and x-ray polarizations by a factor of five or so relative to the parallel case.

Acknowledgments
We would like to thank D A Arms, D L Ederer, E C Landahl and S T Pratt for their assistance with some of the experiments. This work was supported by the Office of Basic Energy Sciences, Office of Science, U.S. Department of Energy, under Contract No. DE-AC02-06CH11357. C Buth was partly supported by the Alexander von Humboldt Foundation.

References

[1] Attwood D 2000 *Soft X-Rays and Extreme Ultraviolet Radiation* (Cambridge: Cambridge University Press)
[2] Als-Nielsen J and McMorrow D 2001 *Elements of Modern X-Ray Physics* (Chichester: Wiley)
[3] Wuilleumier F J and Meyer M 2006 *J. Phys.* B **39** R425
[4] Yamanouchi K 2002 *Science* **295** 1659
[5] Delone N B and Krainov V P 2000 *Multiphoton Processes in Atoms* (Berlin: Springer)
[6] Stapelfeldt H and Seideman T 2003 *Rev. Mod. Phys.* **75** 543
[7] Young L, Arms D A, Dufresne E M, Dunford R W, Ederer D L, Höhr C, Kanter E P, Krässig B, Landahl E C, Peterson E R, Rudati J, Santra R and Southworth S H 2006 *Phys. Rev. Lett.* **97** 083601
[8] Höhr C, Peterson E R, Rohringer N, Rudati J, Arms D A, Dufresne E M, Dunford R W, Ederer D L, Kanter E P, Krässig B, Landahl E C, Santra R, Southworth S H and Young L 2007 *Phys. Rev.* A **75** 011403(R)
[9] Hertlein M P, Adaniya H, Amini J, Bressler C, Feinberg B, Kaiser M, Neumann N, Prior M H and Belkacem A 2006 *Phys. Rev.* A **73** 062715
[10] Santra R, Dunford R W and Young L 2006 *Phys. Rev.* A **74** 043403
[11] Loh Z H, Khalil M, Correa R E, Santra R, Buth C and Leone S R 2007 *Phys. Rev. Lett.* **98** 143601
[12] Pan L, Beck D R and O'Malley S M 2005 *J. Phys.* B **38** 3721
[13] Buth C and Santra R 2007 *Phys. Rev.* A **75** 033412
[14] Buth C, Santra R and Young L 2007 *Phys. Rev. Lett.* **98** 253001
[15] Manson S T and Cooper J W 1968 *Phys. Rev.* **165** 126
[16] Shirley J H 1965 *Phys. Rev.* **138** B979
[17] Chen M H, Crasemann B and Mark H 1980 *Phys. Rev.* A **21** 436
[18] Schmidt V 1997 *Electron spectrometry of atoms using synchrotron radiation* (Cambridge: Cambridge University Press)
[19] Harris S E, Field J E and Imamoğlu A 1990 *Phys. Rev. Lett.* **64** 1107
[20] Boller K J, Imamoğlu A and Harris S E 1991 *Phys. Rev. Lett.* **66** 2593
[21] Fleischhauer M, Imamoğlu A and Marangos J P 2005 *Rev. Mod. Phys.* **77** 633
[22] Szabo A and Ostlund N S 1996 *Modern Quantum Chemistry* (Mineola, NY: Dover)
[23] Clay J T, Walters E A, Grover J R and Willcox M V 1994 *J. Chem. Phys.* **101** 2069
[24] Haack N, Ceballos G, Wende H, Baberschke K, Arvanitis D, Ankudinov A L, and Rehr J J 2000 *Phys. Rev. Lett.* **84** 614
[25] Adachi J, Kosugi N and Yagishita A 2005 *J. Phys.* B **38** R127
[26] DALTON, a molecular electronic structure program, Release 2.0 (2005), see http://www.kjemi.uio.no/software/dalton/dalton.html
[27] Kroto H W 2003 *Molecular Rotation Spectra* (Mineola, NY: Dover)
[28] Hamilton E, Seideman T, Ejdrup T, Poulsen M D, Bisgaard C Z, Viftrup S S and Stapelfeldt H 2005 *Phys. Rev.* A **72** 043402
[29] Kumarappan V, Viftrup S S, Bisgaard C Z, Holmegaard L and Stapelfeldt H 2006 *J. Chem. Phys.* **125** 194309